

Florida Institute of Technology

Scholarship Repository @ Florida Tech

Theses and Dissertations

7-2022

Propellant Optimization for a Pulsed Solid Propellant Thruster System for Small Satellites

Timothy Aaron Blackman

Follow this and additional works at: <https://repository.fit.edu/etd>



Part of the [Aerospace Engineering Commons](#)

Propellant Optimization for a Pulsed Solid Propellant Thruster System for Small Satellites

by

Timothy Aaron Blackman

A thesis submitted to the College of Engineering and Science of
Florida Institute of Technology
in partial fulfillment of the requirements
for the degree of

Master of Science
in
Aerospace Engineering

Melbourne, Florida
July, 2022

We the undersigned committee hereby approve the attached thesis,
“Propellant Optimization for a Pulsed Solid Propellant Thruster System for Small
Satellites.”

by
Timothy Aaron Blackman

Markus Wilde, Ph.D.
Associate Professor
Aerospace, Physics and Space Sciences
Major Advisor

Mark Archambault, Ph.D.
Associate Professor and Assistant Dean of Academics
Aerospace, Physics and Space Sciences

Gerald Micklow, Ph.D.
Professor
Mechanical and Civil Engineering

David Fleming, Ph.D.
Associate Professor and Department Head
Aerospace, Physics and Space Sciences

Abstract

Title: Propellant Optimization for a Pulsed Solid Propellant Thruster System for Small Satellites

Author: Timothy Aaron Blackman

Advisor: Markus Wilde, Ph.D.

CubeSats have historically been used mostly for education, technology demonstration, remote sensing, and amateur radio relay applications. Yet with increased maneuvering capability, they can become effective tools in on-orbit servicing and space debris removal. To make this a reality, CubeSats must be enabled to perform effective rendezvous and proximity operations with non-cooperative client objects, requiring a high-thrust propulsion system. As CubeSats are inherently constrained in their volume and mass, any propulsion system must feature a high specific impulse to minimize the propellant mass requirement. As CubeSats are commonly launched as secondary payload, the use of pressurized propellant tanks is typically ruled out due to concerns about the safety of the primary launch payload. One potential way of accomplishing this combination of high thrust, high specific impulse, and propellant safety is to base the propulsion system on electric on-demand combustion of solid propellant pellets. This thesis uses computational fluid dynamics to identify combinations of propellant chemistry, combustion chamber size, and ignition power resulting in an effective combination of thrust, specific impulse, and total impulse. The software package Flow-3D® was used to perform the simulations for this thesis. This thesis found that the combination of a 50/50 Nitroglycerin/Nitrocellulose propellant in a spherical combustion chamber with high power applied to the Nichrome wire ignitor produces the highest thrust, specific impulse, and total impulse out of all of the combinations.

Table of Contents

Abstract.....	iii
List of Figures.....	vi
List of Tables	viii
Acknowledgement	ix
Dedication.....	x
Chapter 1 Introduction.....	1
Thesis Background and Motivation	1
Thruster Overview.....	1
Thesis Objectives	2
Chapter 2 State of the Art	3
Propellants.....	3
Solid Propellant Modeling.....	5
Chapter 3 Flow-3D® Model.....	8
Combustible Objects Model.....	8
Chapter 4 Simulation Results	16
Initial Conditions.....	16
Meshing and Boundary Conditions.....	18
Thruster Calculations	21
Simulation Results.....	24
Chapter 5 Conclusion	40
Conclusion.....	40
Recommendations/Future Work.....	40

References	41
Appendix	43
Matlab Code	43
Example Matlab Input File Data (80/20 AP/HTPB)	45

List of Figures

Figure 1: GLOBAL Tab	9
Figure 2: PHYSICS Tab	10
Figure 3: FLUIDS Tab.....	10
Figure 4: HEAT TRANSFER Settings.....	11
Figure 5: GEOMETRY Tab	12
Figure 6: COMBUSTING OBJECT PROPERTIES Settings	13
Figure 7: Enabled FSI DEFORMABLE COMPONENT	15
Figure 8: Mesh Structure	19
Figure 9: Propellant Combustion Pressure Over Time	25
Figure 10: Propellant Combustion Temperature Over Time	25
Figure 11: Propellant Thrust.....	26
Figure 12: Propellant Specific Impulse	26
Figure 13: Propellant Total Impulse	27
Figure 14: Change in Adiabatic Combustion Pressure Over Time.....	29
Figure 15: Change in Adiabatic Combustion Temperature Over Time.....	29
Figure 16: Volume Change in Combustion Pressure Over Time	30
Figure 17: Volume Change in Combustion Temperature Over Time	31
Figure 18: Volume Change in Thrust	31
Figure 19: Volume Change in Specific Impulse.....	32
Figure 20: Volume Change in Total Impulse	32
Figure 21: Aspect Ratio Change in Combustion Pressure Over Time	33
Figure 22: Aspect Ratio Change in Combustion Temperature Over Time.....	34
Figure 23: Aspect Ratio Change in Thrust	34
Figure 24: Aspect Ratio Change in Specific Impulse.....	35
Figure 25: Aspect Ratio Change in Total Impulse	35
Figure 26: Power Change in Combustion Pressure Over Time	36
Figure 27: Power Change in Combustion Temperature Over Time	37
Figure 28: Power Change in Thrust.....	37

Figure 29: Power Change in Specific Impulse	38
Figure 30: Power Change in Total Impulse	38

List of Tables

Table 1: Propellant Combusting Object Properties	17
Table 2: Mesh Grid Study Results.....	20
Table 3: Propellant Critical Chamber Pressure.....	27

Acknowledgement

I would like to thank Dr. Wilde for his support in helping me to solve this optimization problem and in seeing it through to the end. I would also like to thank the Senior Design Team SPARCC for allowing me to work alongside them and compare our results with one another. Last, I want to thank Tahir Kanchwala for helping to design the CubeSat thruster system and for initial work on this problem.

Dedication

This thesis is dedicated to both of my parents. They taught me to always keep pushing and to never give up, no matter the odds. Without their support, I would not have the dream of looking to the stars and helping develop our space propulsion technology.

Chapter 1

Introduction

Thesis Background and Motivation

CubeSats are currently often used for various research topics. These topics range from space exploration to aiding Earth-based technologies. Throughout and during the mission profile, the CubeSat adjusts its orbit and stays aligned with the Earth via thrusters, magnetorquers, etc. These adjustments do not require high thrust or maneuverability as the CubeSat does not need to interact with other objects to complete its mission. CubeSats, however, do not have to be confined to research missions as they have the potential to be used for space debris removal, on-orbit servicing, in-space assembly, and other similar missions.

Currently, CubeSats cannot perform missions requiring maneuverability and agility as there is a lack of thrusters that would enable the CubeSat to have high controllability, high thrust, and to move through the space environment safely. Current thruster systems utilize pressurized tanks or require high electrical power. Due to the requirements for launching secondary payloads, CubeSats cannot use pressurized tanks in their propulsion system. Additionally, the use of high electrical power on a small satellite is difficult to achieve as the system needed to meet the power demands reduces the space available for any mission payload. For these reasons, a propulsion concept of using electrically ignited solid propellants was developed by the Florida Tech ORION Lab. This propulsion concept must be characterized to determine the viability for a CubeSat to carry out missions that require it perform rendezvous and proximity operations.

Thruster Overview

The CubeSat thruster is designed to work with one combustion chamber and five nozzles positioned along multiple axes. The nozzles will be used in different combinations

dependent on the required maneuver, giving the CubeSat the ability to move in all six degrees of freedom. The propellant used in the thruster will be stored as small spherical pellets to allow for storage of multiple pellets. A singular pellet will be released into the combustion chamber and will ignite and combust. During the combustion process, the valves leading to each nozzle will be closed. After the pellet has fully combusted and the combustion pressure and temperature have built up within the chamber, one or more valves will open, and the gases will escape through those particular nozzles. The escape of the combustion gases through the nozzles produce thrust and moves the CubeSat through space.

Thesis Objectives

This thesis seeks to identify a combination of propellant, combustion chamber size, and power required resulting in an optimized combination of thrust, specific impulse, and total impulse for a CubeSat thruster. This thesis shall do so through the use of the Flow-3D® modeling software. This thesis is also written in conjunction with the results of the Senior Design team SPARCC who have manufactured the combustion chamber modeled in this research.

Chapter 2

State of the Art

Propellants

Solid propellants have been used for propulsion longer than liquid propellants and continue to be used today. The earliest known use for solid propellants was the use of gunpowder in the Chinese Fire-Arrows around 1232 AD [1]. As technology and weapons improved, gunpowder shifted towards entertainment through the creation of fireworks. Around the 17th century, solid propellants then began to be used as modern rockets. By the 1900s, however, scientists began believing that using liquid propellants in rockets would allow them to fly higher and faster because they produce higher exhaust velocities than solid propellants. This concept would not be realized until 1926 when Robert Goddard first used liquid propulsion in his rockets [1]. Today, solid propellants are used by rocket boosters, rockets, and various weapons. Typical solid propellants used today on small rockets are ammonium perchlorate hydroxyl-terminated polybutadiene (AP/HTPB), nitroglycerine-nitrocellulose, boron potassium nitrate, and gunpowder. Interest in solid propellants is increasing again as they can be used for small satellites and CubeSats.

There are multiple properties of solid propellants that must be considered when choosing which one to use for propulsion. These properties are the burning rate, ignition and combustion temperature, and fuel-oxidizer ratio. The ignition and combustion temperatures determine the ignition delay for the propellants while the fuel-oxidizer ratio impacts the thrust of the propellant. The burning rate is directly impacted by how the propellant is manufactured as well as its density and grain. Smooth propellant grains produce an even burning rate while rough propellant grains disrupt the burning rate. The rough grain creates air pockets and causes the flame to pop, creating uneven burning rates. Thomas et al. [2] study the effect of manufacturing and fuel lamina thickness on the burning rate of AP/HTPB propellants. The researchers compared handmaking the pellets with using a machine to make the pellets. In both cases, the pellets were compressed to ensure that high densities were created. The fuel lamina thickness, layer of fuel, was also varied for both

processed pellets. The comparison found that each method of manufacturing produced similar burning rates; hence, density has more impact on the burning rate than how the propellant is manufactured. In terms of the fuel lamina thickness, the authors found and confirmed that for AP/HTPB pellets, a HTPB lamina thickness of around 200 μm produced a maximum global burning rate [2]. In context of this thesis, the propellants to be modeled can be made by hand. The important properties for each propellant are its density and fuel/oxidizer ratio as they impact the burning rate directly.

Research into the geometry of solid propellants has been done by Northway et al. [3] to determine its impact on specific thrust. The researchers used a pulsed plasma thruster to perform calculations on because it uses solid propellants and can be compared to other thrusters. Various propellants and geometries were tested, and their results were examined. Of the propellants tested, sulfur and Bi_2S_3 gave the best specific thrust. To test geometry, a large surface area is needed to increase the ablated mass (burning rate). However, increasing the surface area also increases the distance between the electrodes that ignite the propellant. This increased distance prevents the propellant from igniting as the ignition arc could not be created without increased power to the electrodes. To counteract this phenomenon, the authors created a serrated configuration that allowed the pellet to ignite while giving it a large surface area. Using sulfur to test, Northway et al. [3] found that more serrated points on the propellant geometry resulted in higher specific thrust.

For this thesis, the geometry of the propellant has been previously set by Kanchwala [4] and the SPARCC Senior Design Team. The propellant is pressed into small spherical pellets to allow for the storage and use of multiple pellets throughout the life of the CubeSat. Each pellet is designed to provide enough thrust to move the CubeSat efficiently in space. Moreover, the pellets are small enough to ensure that small adjustments can be made without burning through the supply of propellant. Each propellant pellet has a radius of 3 mm.

Additives can be added to the propellants to further improve the performance [5, 6]. Dillier et al. [5] tested by adding varying amounts of boron and aluminum to AP/HPTB propellants. The authors found that adding 0.15% boron and 0.60% aluminum to the pellets

increases the burning rate significantly. This particular ratio generated the highest burning rate out of all of the other ratios tested [5]. He et al. [6] specifically tested electrically controlled solid propellants (ECSPs) in their research. The researchers found that by adding aluminum powder to the propellants, their tensile strength and initial modulus improved while reducing the propellant elongation. This improved the propellant grain by creating strong bonds between the atoms in the propellant. He et al. [6] showed the important relationship between the propellant grain and the properties of the propellant.

This thesis does not include any additives in the calculations. This thesis takes the grain of the propellants into account by using their densities in the calculations.

Solid Propellant Modeling

To validate the use of solid propellants for a CubeSat thruster, the combustion process must be modeled and tested. The SPARCC team has successfully manufactured the combustion chamber and nozzle for the CubeSat thruster. This thruster model, however, is only good for one combustion chamber size and nozzle. To effectively validate the use of solid propellants, the combustion process must be modeled using computational fluid dynamics (CFD) so that various chamber sizes and other parameters can be altered to find the optimal combination for the CubeSat.

Various CFD software tools were examined for use in this thesis: Ansys Fluent, OpenFOAM and Flow-3D®.

Ansys Fluent (Fluent) has various solvers that it uses to solve problems. The majority of the problems deal with particle flows or with some other flow that has already been established. Ansys Fluent has a coal combustion solver [7]. However, this solver is optimized only for coal and cannot substitute in any other solid propellant. Al Mayas et al. [8] and other researchers instead input the combustion gases and products from the solid propellant into Ansys Fluent and use those values to compute the flow parameters. Ansys Fluent does have a multiphase flow solver, which Bougamra and Lu used to simulate the

solid propellant combustion in a small gun chamber [9]. However, Bougamra and Lu assume perfect ignition and did not simulate the ignition of the solid propellant. The perfect ignition assumption was that the propellant began to burn in the entire chamber volume at zero seconds. Moreover, the Ansys Fluent materials database does not contain AP/HTPB or other standard solid propellants for rockets. While the ability to create new materials is included in Fluent, very little properties for each solid propellant could be found and the propellant could not be entered into the system. Additionally, Fluent uses a Scheme file format for its materials while NASA JANAF tables utilize their own format. This prevented the use of inputting NASA tables into Ansys Fluent. Converting the NASA tables to Fluent proved difficult as converters and tutorials could not be found. Ultimately, the solid combustion model could not be replicated in Ansys Fluent with the desired propellants.

OpenFOAM has the same limitations as Ansys Fluent. OpenFOAM has a coal combustion solver but is optimized for only coals. OpenFOAM also has a multiphase flow and other reacting flow solvers [10]. As with Fluent, other researchers have used OpenFOAM to model the combustion gases of the solid propellants without modeling the combustion process itself [11,12]. Yet, the pyrolysis of HTPB can be modeled in OpenFOAM to show its combustion process [13]. However, the OpenFOAM library also does not include standard solid propellants and uses a different format for its materials than NASA does. Additionally, OpenFOAM uses CHEMKIN [10] to calculate the chemical kinetics and reactions of its materials, which is a different file format to the thermodynamic tables that NASA uses. Consequently, solid combustion could also not be modeled in OpenFOAM.

Upon further research, the Flow-3D® CFD software was found [14]. Flow-3D® has many of the same solvers that Fluent and OpenFOAM both have, yet Flow-3D® has a combustible objects model that distinguishes it from all other commercial CFD software packages. With this solver, Flow-3D® is able to model the combustion process of a solid propellant. Unlike Fluent or OpenFOAM, Flow-3D® bases its combustion process on the density, ignition and combustion temperatures, and burning rate of the solid propellants. With Fluent and OpenFOAM, researchers must hard code in the combustion process for

solid propellants as they do not have a native solver for this process, whereas Flow-3D® natively solves for the solid combustion process and allows the user to input any material without the need for a database or CHEMKIN file. For these reasons, Flow-3D® was selected and used as the CFD modeling software for this thesis. The full version of Flow-3D® was not able to be purchased and used, instead, the academic version was used to complete each test.

Chapter 3

Flow-3D® Model

Combustible Objects Model

This chapter is designed to allow the reader to be able to recreate the simulation of solid combustion.

When creating a NEW SIMULATION, the units are set for that simulation. The units can either be the International System of Units (SI), the Centimeter-Gram-Second System of Units (CGS), the English Engineering Units (ENGINEERING), or a Custom System of Units (CUSTOM). This thesis used the CUSTOM units setting by changing the SI unit of length to centimeters and keeping the SI units of mass, time, and temperature the same SI units. Each simulation is then first set up through the GLOBAL tab. This first tab sets the PRESSURE TYPE, the REFERENCE PRESSURE, the REFERENCE TEMPERATURE, and the START AND FINISH CONDITIONS. The PRESSURE TYPE was set to ABSOLUTE so that the calculated pressures would be formatted as absolute pressures. The REFERENCE PRESSURE was set to $1013 \text{ kg/cm} \cdot \text{s}^2$ (1 atm) and the REFERENCE TEMPERATURE was set to 273.15 K. The REFERENCE PRESSURE and REFERENCE TEMPERATURE sets the ambient and initial conditions for the simulation. The FINISH TIME was set to 7 seconds for each propellant test except for the 50/50 Nitroglycerine/Nitrocellulose propellant. The 50/50 Nitroglycerine/Nitrocellulose propellant was set to 2 seconds because the combustion process was found to have completed within that time. The GLOBAL TAB is shown in Figure 1.

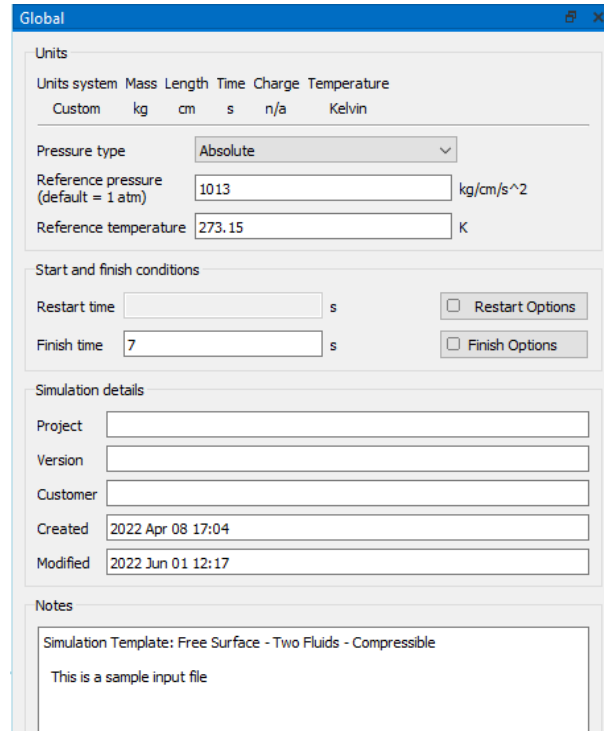


Figure 1: GLOBAL Tab

To use the Combustible Objects Model in Flow-3D®, the flow mode must be set to COMPRESSIBLE in the PHYSICS tab, as seen in Figure 2 [15]. Setting the flow mode to COMPRESSIBLE causes the software to use two fluids when it solves the flow conditions and also enables the use of the Combustible Objects Model. The Fluid 1 and Fluid 2 properties are set in the FLUIDS tab, as shown by Figure 3. For this thesis project, Fluids 1 and 2 were both defined as air as the model was built for in-atmosphere simulations. Fluid 2 is where the products of the solid combustion go and is how the data for the simulation can be accessed. In addition to the COMPRESSIBLE flow mode, the DENSITY EVALUATION, HEAT TRANSFER, and VISCOSITY AND TURBULENCE models must be turned on. Each solution model is also seen in Figure 2. Turning on the Combustible Objects Model automatically turns on these models. The default settings for each of these models, except for heat transfer, were used in this paper.

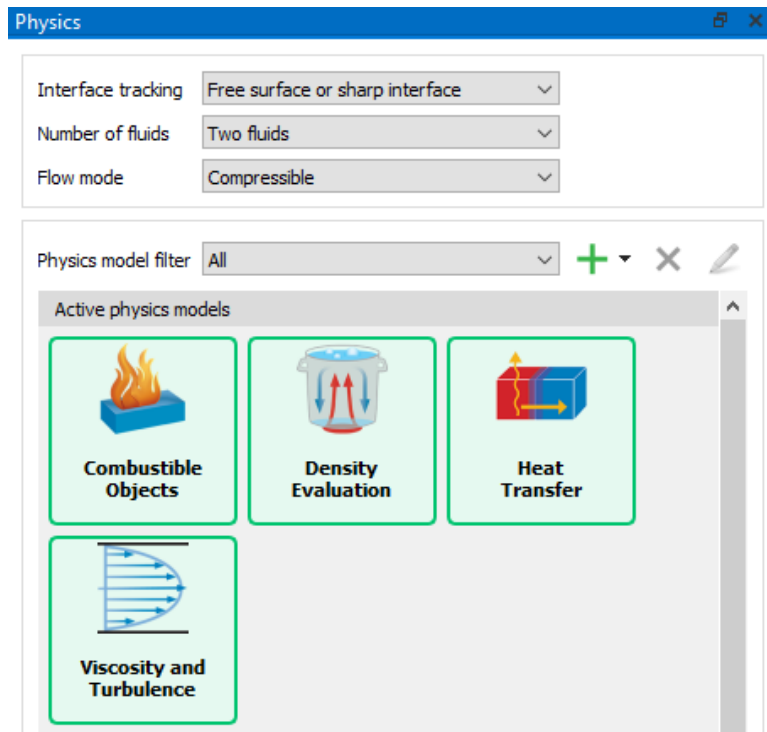


Figure 2: PHYSICS Tab

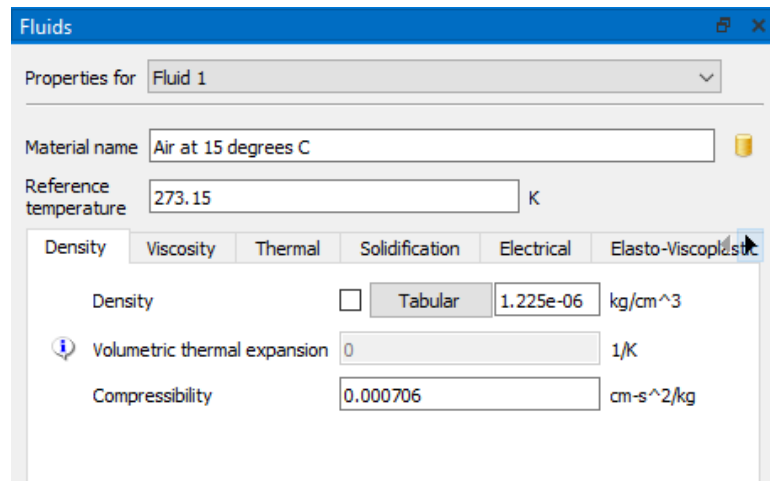


Figure 3: FLUIDS Tab

In the heat transfer model, the FLUID TO SOLID HEAT TRANSFER option was turned on as shown in Figure 4. This option enabled both the ability to create a Nichrome wire within the problem and the ability to model the heat transfer between the combustion gases and the chamber walls. The Nichrome wire and combustion chamber properties were set in the GEOMETRY tab as seen in Figure 5. The heat transfer mode, thermal conductivity, density and specific heat, heat source, and total amount of power settings are found under the SOLID PROPERTIES settings in the COMPONENT PROPERTIES tab. The heat source and total amount of power were set for the wire as it is the ignitor. To model full heat transfer to the combustion chamber and from the wire, the thermal conductivity, density, and specific heat were defined. The full heat transfer is modeled as conduction.

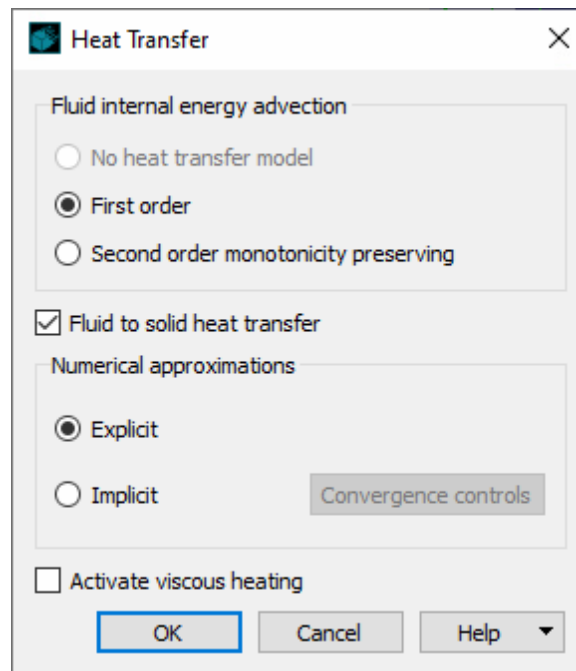


Figure 4: HEAT TRANSFER Settings

Geometry

Objects Status Color Type

▼ Nichrome	<input checked="" type="checkbox"/>			General (Solid)
Nichrome	<input checked="" type="checkbox"/>			Solid

Component Properties Nichrome

Material

Combusting Object Properties
Dissolving Object Properties
FSI Deformable Properties
Initial Conditions
Mass Source Properties
Solid Properties
Squeeze Pin Properties
Surface Properties
Thermal Stress Properties

Heat transfer mode

Thermal conductivity ☐ Temperature kg-cm/s³/K

Thermal conductivity multipliers

X-direction

Y-direction

Z-direction

Density*Specific heat ☐ Temperature kg/cm/s²/K

Heat source

Type

Total amount ☐ Time kg-cm²/s³

Specific amount ☐ Time kg/cm/s³

Control type

On/Off status ☒ Time

Thermocouple

Turn on temperature K

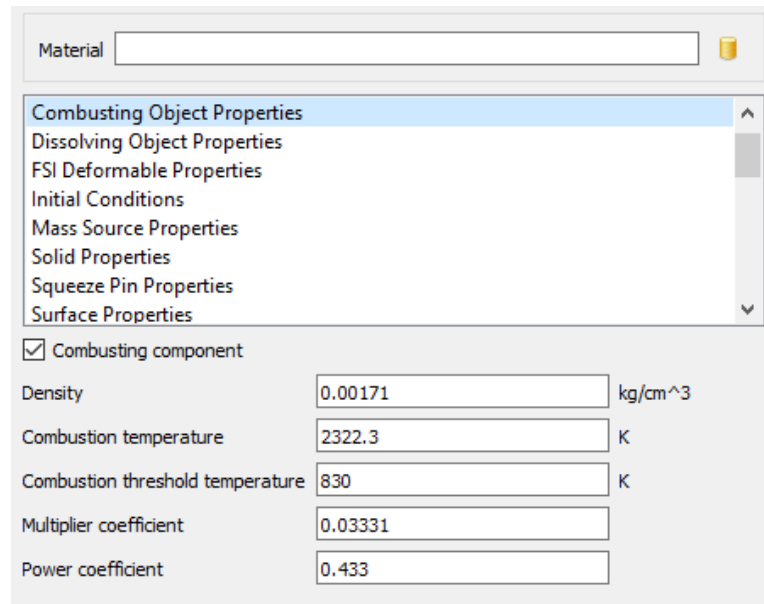
Turn off temperature K

Maximum thermal penetration depth ☐ cm

Shell mold

Figure 5: GEOMETRY Tab

Like the Nichrome wire, the combustible objects data is input in the GEOMETRY tab of the GUI, as displayed by Figure 6. The data shown in Figure 6 is of the 80/20 AP/HTPB propellant. When defining the propellant in the software, the propellant must be of the type SOLID, and its properties are set in the COMBUSTION OBJECT PROPERTIES under the COMPONENT PROPERTIES tab. The parameters that Flow-3D® uses to solve the problem are the density, combustion temperature, combustion threshold temperature (ignition temperature), multiplier coefficient (burning rate), and power coefficient (burning rate coefficient). Flow-3D® does not model the chemistry of the reaction; instead, the reaction is modeled by the combustion rate and its empirical coefficients. These values are obtained from previous experiments.



Property	Value	Unit
Density	0.00171	kg/cm ³
Combustion temperature	2322.3	K
Combustion threshold temperature	830	K
Multiplier coefficient	0.03331	
Power coefficient	0.433	

Figure 6: COMBUSTING OBJECT PROPERTIES Settings

According to the User Manual [15], Flow-3D® solves for combustion through converting the solid material into a fluid via a mass transfer rate Q_M :

$$Q_M = \rho_{solid} a \quad (1)$$

Equation (1) shows the formula used to solve for the mass transfer rate, where ρ_{solid} is the propellant density, and a is the multiplier coefficient. According to the manual, a is the normal speed of the propellant or in other words, the burning rate [15]. The burning rate must be found empirically from past experiments. As shown in equation (2), the solver then finds the energy Q_E produced by the reaction using the combustion mass flow rate.

$$Q_E = Q_M C_p T_{burn} \quad (2)$$

In this formula Q_E is the energy produced by the reaction, C_p is the specific heat capacity at constant pressure, and T_{burn} is the combustion temperature of the propellant as given by previous experiments. The propellant is assumed to be stagnant which eliminates the need for additional source terms in the momentum equations used by the solver. The solver then uses a Flow-3D® specific object representation known as the Fractional Area/Volume Obstacle Representation (FAVOR™) to show the changing propellant geometry. FAVOR™ calculates the changing volume within a mesh cell and then calculates the amount of burned propellant through integration of equation (3).

$$dM = Q_M dA dt \quad (3)$$

In equation (3), dA is the surface area of the propellant in the mesh cell. These equations in addition to mass, energy, and momentum sources are used by the combustible objects model to solve for combustion.

The last setting to enable is the FSI DEFORMABLE PROPERTIES under the COMPONENT PROPERTIES as seen in Figure 7. This setting is used to mesh the propellant itself and allows the solver to deform the propellant. To use this setting, the propellant must be turned off as a combustible object momentarily. The FSI (Fluid Structure Interaction) deformable properties can then be turned on and the mesh for the propellant can be made. After the mesh is created, the FSI deformable properties must be turned off and the combustible object properties turned back on for the solver to work properly again.

Axisymmetric Spinning Object Properties
 Combusting Object Properties
 Dissolving Object Properties
FSI Deformable Properties
 Initial Conditions
 Mass Source Properties
 Solid Properties
 Squeeze Pin Properties

☒ FSI deformable component

Solid density ☐ Temperature kg/cm³

Volumetric thermal expansion 1/K

Elastic properties

Compute from Elastic modulus and Poisson's ratio

Elastic modulus ☐ Temperature kg/cm/s²

Poisson's ratio ☐ Temperature

Yield stress ☐ Temperature kg/cm/s²

FSI coupling between Propellant and:

Fluid Partial


 FSI components required to defined component interactions

Figure 7: Enabled FSI DEFORMABLE COMPONENT

Chapter 4

Simulation Results

Initial Conditions

As mentioned in Chapter 3, the data needed to simulate solid combustion are propellant density, ignition and combustion temperatures, burn rate, and the burn rate exponent. To also model the heat transfer to the propellant, the specific heat and thermal conductivity of the propellant must also be found. The propellants that were simulated are AP/HTPB, Nitrocellulose/Nitroglycerin, and BKNO_3 . The AP/HTPB was simulated at 80% AP and 20% HTPB, and 70% AP and 30% HTPB. The Nitrocellulose/Nitroglycerine was simulated at 50%/50%. Surprisingly, there are but few research papers and databases that contain all of the necessary data in one place. Consequently, the necessary values were found from various sources to simulate the combustion for each propellant. Table 1 summarizes these values.

Table 1: Propellant Combusting Object Properties [4,16–22]

Propellant	70/30 AP/HTPB	80/20 AP/HTPB	50/50 Nitroglycerin/Nitrocellulose	BKNO3
Density (kg/m ³)	1615	1710	1600	1400
Combustion Temperature (K)	1400	2322.3	3220	2890
Ignition Temperature (K)	830	830	474.25	830
Burn Rate (m/s)	$3.33 \cdot 10^{-4}$	$3.33 \cdot 10^{-4}$	$8.00 \cdot 10^{-4}$	$3.81 \cdot 10^{-4}$
Burn Rate Exponent	0.433	0.433	0.7	0.306
Specific Heat (J/kg·K)	1880	1740	1673.6	6740.7
Thermal Conductivity (W/m·K)	$4.02 \cdot 10^{-5}$	$4.02 \cdot 10^{-5}$	$2.14 \cdot 10^{-5}$	$1.40 \cdot 10^{-5}$

The combustion chamber is modeled to be of Stainless Steel 304, matching the combustion chamber prototype by the SPARCC team. The properties that Flow-3D® needs to calculate the heat transfer from the combustion gases to the chamber are the density, specific heat, and thermal conductivity of the chamber. The density of stainless steel 304 is 7930 kg/m³, the specific heat is 500 J/kg·K, and the thermal conductivity is 16.2 W/m·K [23].

The Nichrome wire is a Nichrome 80, 20 gage with an average diameter of 0.032 inches [24]. Flow-3D® needs the density, specific heat, thermal conductivity, and power since it is the heat source in the problem. The Nichrome has a density of 8418 kg/m³, specific heat of 460 J/kg·K, and thermal conductivity of 11.3 W/m·K [25]. Equation (4) was used to solve for the electrical power heating the wire.

$$P = \frac{V^2}{R} \quad (4)$$

In this equation, P is the power, V is the voltage, and R is the wire resistance. For the simulations 9 volts were applied to the wire, which resulted in 128 W of heat load. The wire was set at an initial temperature of 1298.15 K, which is well under its melting point [24].

Meshing and Boundary Conditions

To reduce computational time and resources, two meshes were created within each simulation. The first mesh contains the entirety of the combustion chamber, Nichrome wire, and propellant while the second mesh contains only the propellant and Nichrome wire. The first mesh is coarser than the second by a factor of 10. This created less cells throughout the combustion chamber and concentrated more cells around the propellant, decreasing computation time and increasing computational efficiency. Figure 8 displays the typical mesh set up for each simulation.

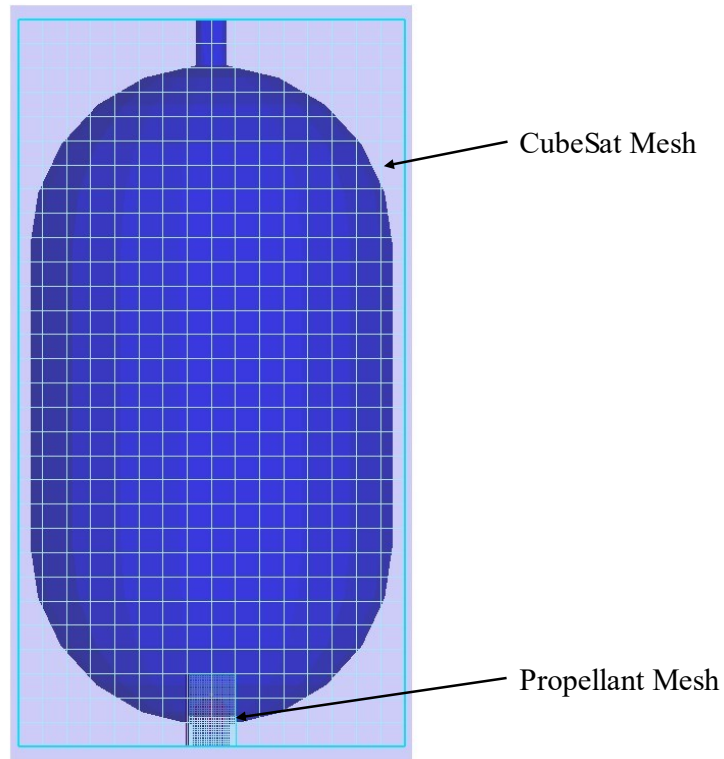


Figure 8: Mesh Structure

A grid study was performed to ensure that the coarse CubeSat mesh would provide accurate results. The grid study compared the mesh size used in each simulation to three finer meshes. The mesh size, as seen in Figure 8, has cell sizes of 0.4 cm while the finer meshes had cell sizes of 0.25 cm, 0.20 cm, and 0.18 cm. The same initial and boundary conditions used in the 80% AP, 20% HTPB propellant test were used as well as the 80/20 AP/HTPB propellant to compare the grid results. The results for each mesh are given in Table 2.

Table 2: Mesh Grid Study Results

Test	Cell Size (cm)	Thrust (N)	Specific Impulse (s)	Total Impulse (N-s)
Coarse	0.40	2.71	51.42	0.096
Fine	0.25	3.31	51.25	0.097
Finer	0.20	2.84	42.90	0.081
Finest	0.18	2.92	44.79	0.085

As the grid mesh decreases in cell size, the computational time increases. The coarse grid completed in four hours while the finest mesh completed in 65 hours. As the academic version of Flow-3D® is used to complete these tests, only one simulation can run at a time. Considering these computational times along with the differences between thrust, specific impulse, and total impulse for each test, the coarse mesh was used throughout this thesis in order to reduce computational time and increase computational efficiency. Future work can be done in order to obtain the full version of Flow-3D® so that more tests can be simulated at the same time and allow for more accurate results.

The boundaries of the combustion chamber cut through the mesh cells. Flow-3D® solves this issue by using FAVOR™ to model the curved edges of the combustion chamber. The combustion chamber is also set as a COMPLEMENT solid, which tells the software to combust the solid propellant within the geometry. Using both of these settings, Flow-3D® is able to apply the boundary conditions to the walls of the combustion chamber.

The extents of each mesh are referred to as mesh walls. The boundary conditions for each simulation were placed on the mesh walls. For the walls containing the first mesh, all of the boundaries were set as a wall to simulate the combustion gases staying inside the chamber. This was done because the thruster is designed to let the combustion gases build up and then escape through any nozzle on the CubeSat. This allows for the CubeSat to travel in any direction. For the walls containing the second mesh, every side except for the Y-Maximum wall was set as a wall. The Y-Maximum wall was set to CONTINUATIVE to simulate the combustion gases escaping upward from the pellet. This was done as the

Nichrome wire was placed on top of the propellant, so the gases would escape from the top first. As stated in Chapter 3, the combustion chamber walls are set to the REFERENCE TEMPERATURE of 273.15 K. This temperature is also the ambient temperature for each simulation. The temperature of the chamber walls is then simulated through the conductive heat transfer calculations.

Thruster Calculations

To calculate the thrust, specific impulse, and total impulse of the CubeSat, the combustion gases and the nozzle geometry were used. The calculations are completed for sea-level conditions and the combustion gases are assumed to be ideal, and calorically perfect. The nozzle used is a converging-diverging nozzle with a nozzle half-angle of 8° located on the diverging section. The Flow-3D® simulations output the combustion chamber pressure and temperature, density, and average velocity of the combustion gases based on the properties of the propellant. As calculated by the ideal gas law in equation (5), using the pressure, density, and temperature of the combustion gases gives the specific gas constant (R_g) for the gases.

$$R_g = \frac{p_{comb}}{\rho_{comb} T_{comb}} \quad (5)$$

Equation (6) is one of the relations for any calorically perfect gas. This equation can be rearranged into equation (7), which solves for the specific heat ratio from the specific gas constant and the specific heat capacity for the combustion gases. The specific heat capacity c_p is taken from the propellant data given in Table 1.

$$c_p = \frac{\gamma}{\gamma - 1} R_g \quad (6)$$

$$\gamma = \frac{\frac{c_p}{R_g}}{\frac{c_p}{R_g} - 1} \quad (7)$$

Now the combustion properties can be calculated using the specific heat ratio and the specific gas constant. Using equation (8) the speed of sound can be found within the combustion chamber.

$$a_{cc} = \sqrt{\gamma R_g T_{comb}} \quad (8)$$

The average Mach Number can then be found from the average velocity of the gases and the speed of sound.

$$M_{cc} = \frac{u_{cc}}{a_{cc}} \quad (9)$$

Using compressible flow and assuming isentropic flow, the stagnation pressure and temperature can be found.

$$p_0 = p_{comb} \left(1 + \frac{\gamma-1}{2} M_{cc}^2 \right)^{\frac{\gamma}{\gamma-1}} \quad (10)$$

$$T_0 = T_{comb} \left(1 + \frac{\gamma-1}{2} M_{cc}^2 \right) \quad (11)$$

Despite the low velocities and low Mach Numbers within the combustion chamber, the stagnation pressure and temperature values were calculated to decrease the computational error. The stagnation pressure and temperature will both increase as the combustion process occurs. The rest of the calculations were performed with choked flow at the nozzle throat. The critical pressure ratio was calculated for each propellant to verify the choked flow. Equation (12) is used to find the critical pressure ratio.

$$\frac{p_0}{p_a} \geq \left(\frac{\gamma+1}{2} \right)^{\frac{\gamma}{\gamma-1}} \quad (12)$$

Multiplying the critical pressure ratio by the ambient pressure gives the minimum combustion chamber pressure needed to choke the flow. The nozzle was choked in every test as the combustion chamber pressure exceeded the minimum amount.

The converging-diverging nozzle has a nozzle exit diameter of 5.895 mm while its throat has a diameter of 3.151 mm. Using these diameters, the areas are $2.729 \cdot 10^{-5} \text{ m}^2$ and

$7.798 \cdot 10^{-6} \text{ m}^2$ respectively. Dividing the nozzle area by the throat area gives an area relation which can be used in the area-Mach number relation to solve for exit Mach flow.

$$\frac{A_{noz}}{A^*} = \frac{1}{M_e} \left[\frac{2}{\gamma + 1} \left\{ 1 + \frac{\gamma - 1}{2} M_e^2 \right\} \right]^{\frac{\gamma + 1}{2(\gamma - 1)}} \quad (13)$$

The exit Mach flow can then be used to solve for the static exit pressure and temperature. The static exit pressure is not equal to the atmospheric pressure, causing the flow to either be over-expanded or under-expanded. The flow is over-expanded if the exit pressure is less than the atmospheric pressure and is under-expanded if the exit pressure is greater than the atmospheric pressure. Since a burner is not present in the nozzle and the flow is assumed isentropic, the stagnation pressure and temperature remain the same. The density of the exit flow can also be calculated.

$$p_e = \frac{p_0}{\left(1 + \frac{\gamma - 1}{2} M_e^2 \right)^{\frac{\gamma}{\gamma - 1}}} \quad (14)$$

$$T_e = \frac{T_0}{\left(1 + \frac{\gamma - 1}{2} M_e^2 \right)} \quad (15)$$

$$\rho_e = \frac{p_e}{R_g T_e} \quad (16)$$

Using the exit temperature and exit Mach number, the exit velocity is computed.

$$u_e = M_e \sqrt{\gamma R_g T_e} \quad (17)$$

The exit mass flow rate is calculated through equation (18).

$$\dot{m} = \rho_e u_e A_{noz} \quad (18)$$

Using the nozzle diameter, nozzle half-angle α , and equations (14) – (18), the thrust τ , specific impulse I_{sp} , and total impulse I of the CubeSat thruster can be determined.

$$\tau = \frac{1 + \cos \alpha}{2} (\dot{m} u_e) + (p_e - p_a) A_{noz} \quad (19)$$

$$I_{sp} = \frac{\tau}{\dot{m} g} \quad (20)$$

$$I = I_{sp} * m_p * g \quad (21)$$

For equation (19), p_a is 101,325 Pa as the simulation was performed at sea-level. In equations (20) and (21), g is standard gravity. The mass of the propellant m_p was determined through the volume and density of each spherical propellant. Each pellet had a radius r of 3 mm.

$$V_{prop} = \left(\frac{4}{3}\right) \pi r^3 \quad (22)$$

$$m_p = \rho_{prop} * V_{prop} \quad (23)$$

Simulation Results

This section displays the simulation results from changing propellants, combustion chamber volume, combustion chamber aspect ratio, and Nichrome wire power. The pressure and temperature plots in this section are the average values from the combustion chamber as a result of the combustion process and its heat transfer to the chamber walls. Additionally, for each thrust, specific impulse, and total impulse bar chart, the values are calculated at the end of the full combustion process for each propellant. This ensures that the calculations through the nozzle of the CubeSat are correct because the nozzle was designed to produce supersonic flows only when a pellet has fully combusted.

Figure 9 through Figure 13 display the results of changing the propellant in the combustion chamber. The combustion chamber modeled was the one built by the SPARCC team.

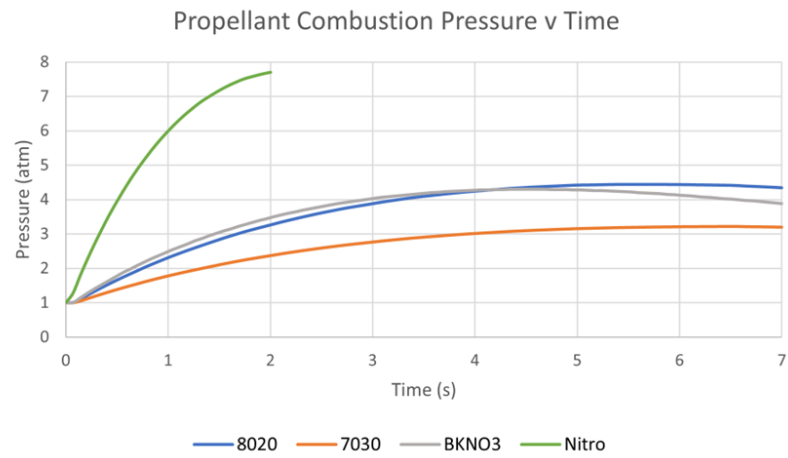


Figure 9: Propellant Combustion Pressure Over Time

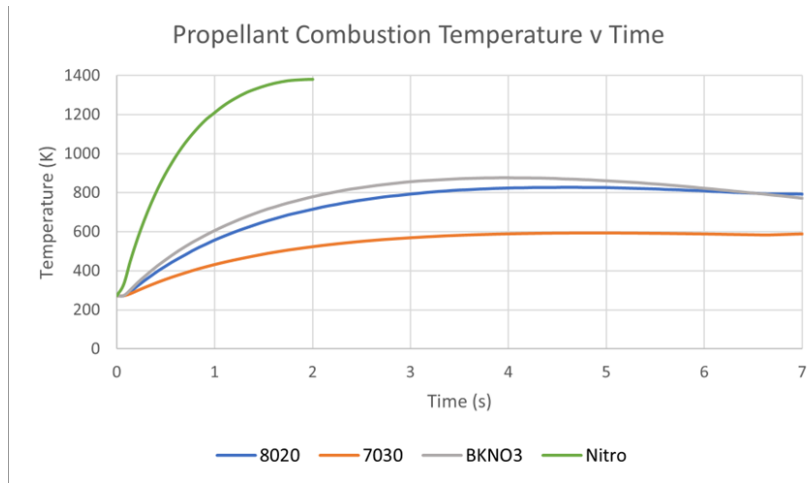


Figure 10: Propellant Combustion Temperature Over Time

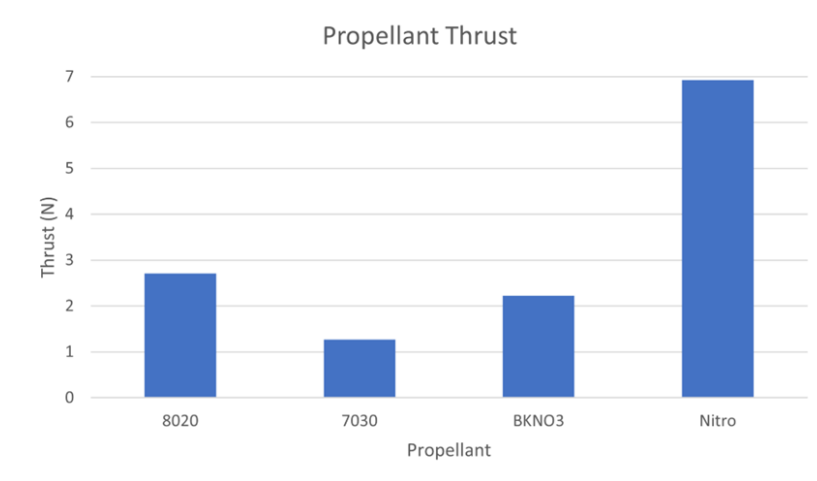


Figure 11: Propellant Thrust

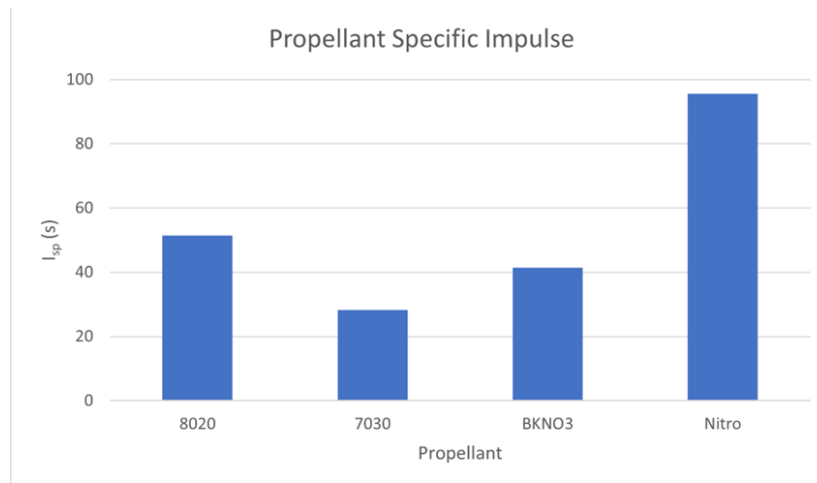


Figure 12: Propellant Specific Impulse

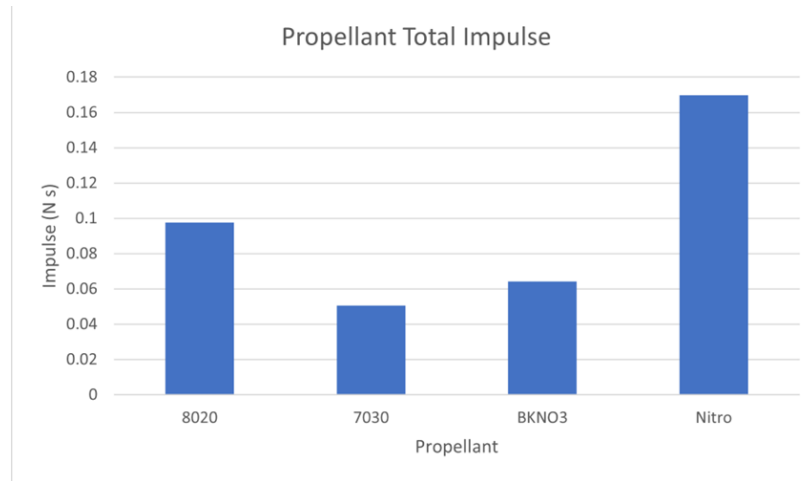


Figure 13: Propellant Total Impulse

As mentioned in the Thruster Calculations Section, the critical chamber pressure is calculated at sea-level and from equation (12). The critical chamber pressures for each propellant are given in Table 3.

Table 3: Propellant Critical Chamber Pressure

Propellant	Critical Chamber Pressure (atm)
80/20 AP/HTPB	1.732
70/30 AP/HTPB	1.726
BKNO ₃	1.663
50/50 Nitroglycerin/Nitrocellulose	1.732

The nozzle will choke at pressures equal and higher than the critical pressures given. Figure 9 shows that the nozzle chokes for each propellant because each chamber reaches higher than the critical chamber pressure. The combustion chamber pressure and

temperature used in the thruster calculations are the very last points on each of the graphs in Figure 9 and Figure 10. These values correspond to opening the valve at that point in time which produces an instantaneous thrust. The values before these points show the combustion chamber pressure and temperature within the closed chamber over the course of the combustion process.

Figure 11, Figure 12, and Figure 13 show that the use of a 50/50 Nitroglycerin/Nitrocellulose (aka 50/50) pellet will produce the highest thrust, specific impulse, and total impulse out of all of the propellants tested. The 50/50 pellet combusts fully within 2 seconds while the other propellants fully combust by 7 seconds. The pressure and temperature figures show this by the 50/50 pellet data ending after 2 seconds. The 50/50 pellet generates over twice the amount of thrust as the 80/20 AP/HTPB pellet in a smaller amount of time. Figure 12 proves that this is possible for the 50/50 propellant as the calculated specific impulse is below the recorded maximum of 230 s. In comparing the specific impulse of the 50/50 propellant with recorded data from Lengellé et al. [17], the calculated specific impulse falls below the recorded maximum value of 230 s. Additionally, the total impulse data displayed in Figure 13 is comparable to the 0.109 N·s calculated value for solid propellants mixed with a Nitrocellulose additive, as recorded by Staley et al [26]. The simulated 50/50 pellet is larger in size than the pellet used by Staley et al [26]. The 50/50 pellet also has Nitroglycerin and Nitrocellulose as the propellant and not as an additive, which accounts for the larger total impulse for the pellet. The reason that this propellant creates so much thrust is seen in Figure 9, where the pressure generated by the combustion gases is nearly twice the pressure generated by the other propellants. Figure 9 and Figure 10 show that the 80/20 AP/HTPB pellet nearly reaches the same pressures and temperatures as the BKNO_3 pellet, which makes their thrust values comparable. Additionally, Figure 9 and Figure 10 depict a decrease in chamber pressure and temperature at the end of the combustion process. This decrease is due to the heat transfer occurring between the combustion gases and combustion chamber walls. The decrease in combustion chamber pressure and temperature is verified in Figure 14 and Figure 15.

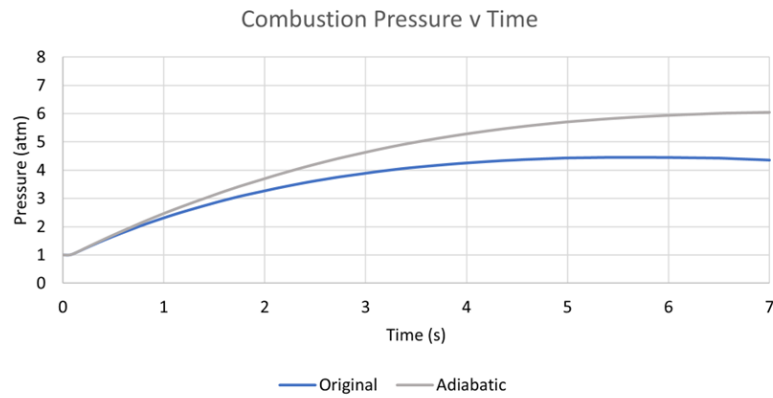


Figure 14. Change in Adiabatic Combustion Pressure Over Time

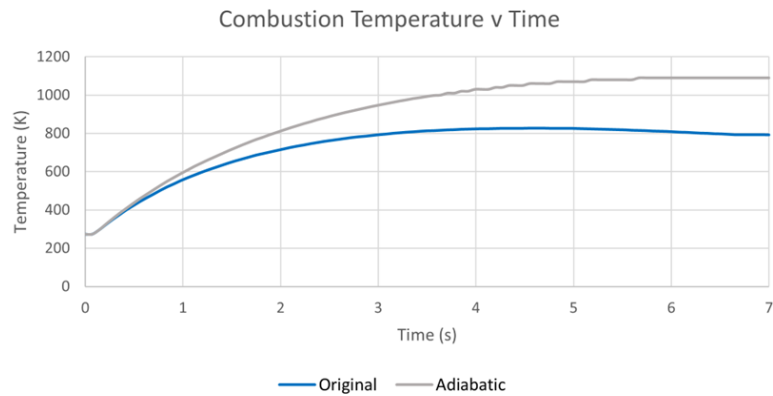


Figure 15. Change in Adiabatic Combustion Temperature Over Time

To verify that the heat transfer causes the reduction of chamber pressure and temperature, an adiabatic test was performed. This test used the 80/20 AP/HTPB pellet and the same initial and boundary conditions as the 80/20 AP/HTPB test did. However, the conductive heat transfer to the combustion chamber walls was turned off for the adiabatic test. Figure

14 displays that the combustion chamber pressure increases and remains constant for the adiabatic case while the pressure increases before decreasing for the heat transfer case. Figure 15 shows the same results for the combustion chamber temperature. As heat transfer is used in each test, the combustion chamber pressure and temperature will decrease for each test.

Figure 16 through Figure 20 show the impact of changing the combustion chamber volume on the thruster performance. The combustion chamber used for these tests is a spherical chamber. For the rest of the tests in this section, an 80/20 AP/HTPB pellet is used. Each test attains pressures higher than the critical pressure for the 80/20 AP/HTPB pellet and thus, the nozzle is choked for each remaining test.

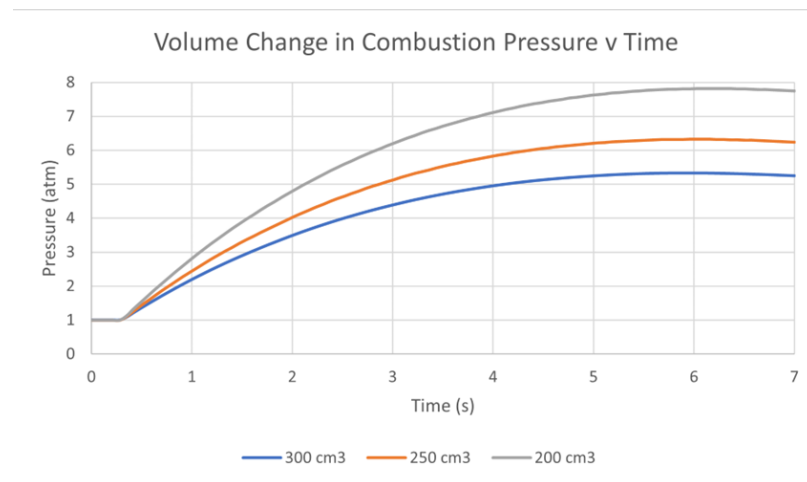


Figure 16: Volume Change in Combustion Pressure Over Time

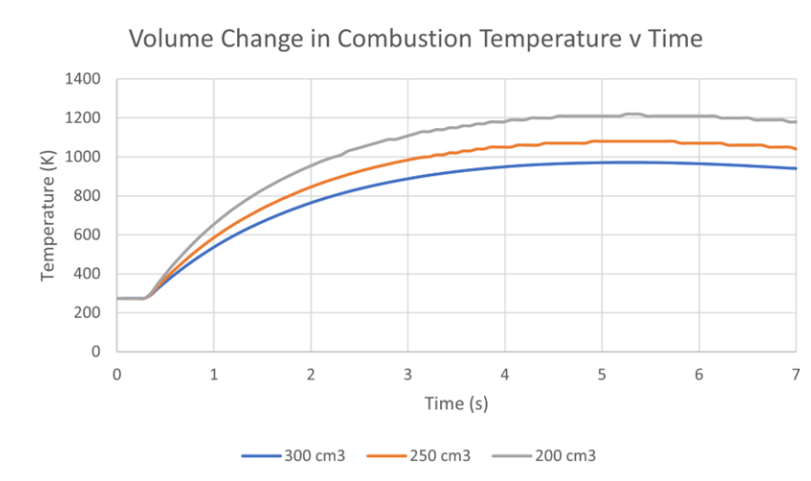


Figure 17: Volume Change in Combustion Temperature Over Time

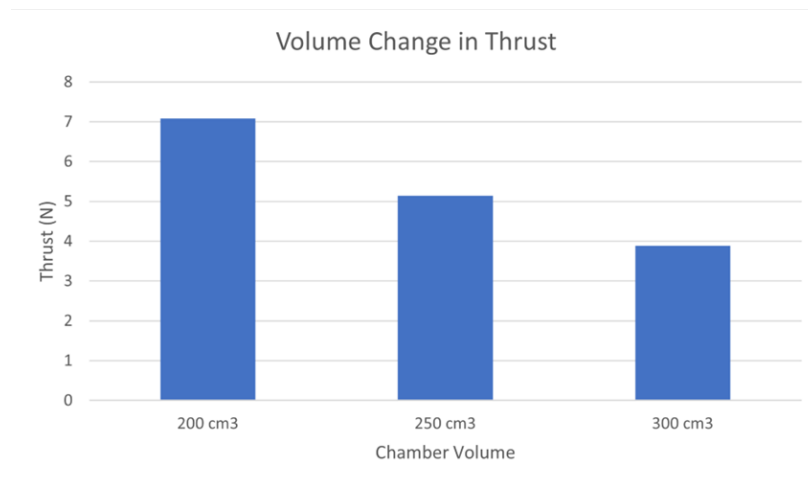


Figure 18: Volume Change in Thrust

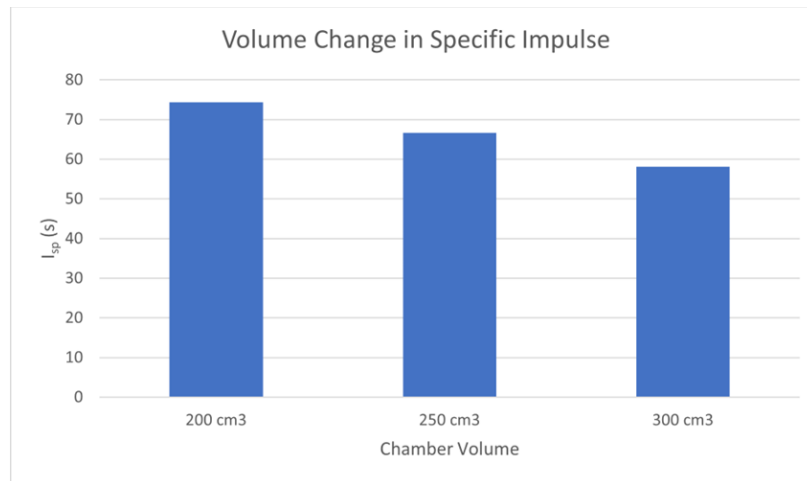


Figure 19: Volume Change in Specific Impulse

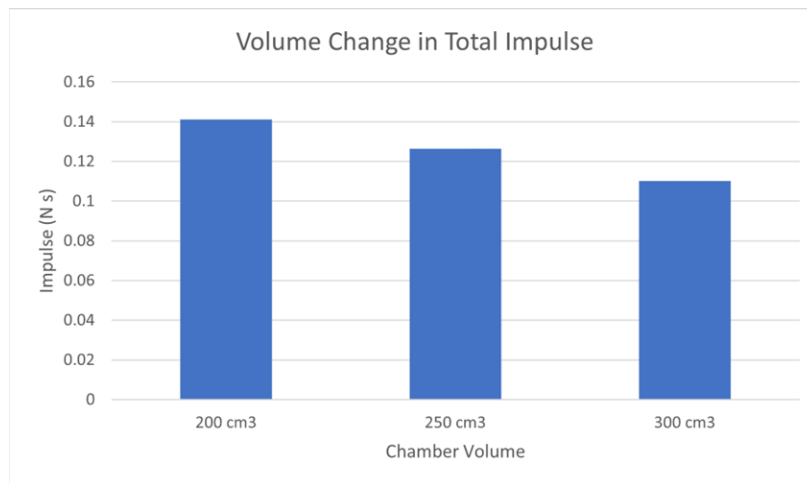


Figure 20: Volume Change in Total Impulse

Figure 18 shows that the higher value of thrust is found at lower combustion chamber volumes. Figure 19 and Figure 20 also show the same trend for specific impulse and total impulse. The reason that the higher thrust and impulses exist for smaller combustion

chamber volumes is because there is less space for the gas to fill. This in turn creates higher pressures, as seen in Figure 16. Figure 17 shows that despite the higher pressure in the chamber, volume does not have as significant of an effect on the combustion temperature. The initial values for both chamber pressure and temperature in both Figure 16 and Figure 17 increase slightly, causing each graph to appear to have constant chamber pressure and temperature. This slight change is lost in the graphs as the overall change in chamber pressure and temperature is large.

Figure 21 through Figure 25 show the effect of changing the aspect ratio on the thruster values. For each test, the combustion chamber is kept at a volume of 200 cm^3 . Each aspect ratio is written in the form of “chamber radius: chamber length” (I.e., 1:3).

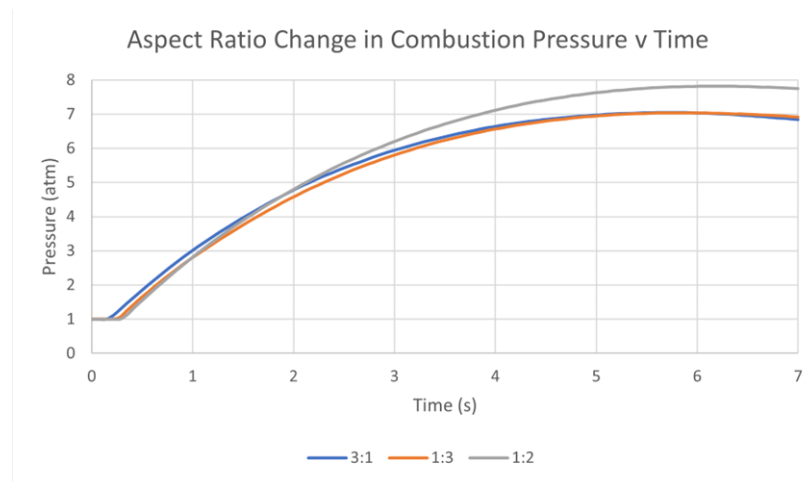


Figure 21: Aspect Ratio Change in Combustion Pressure Over Time

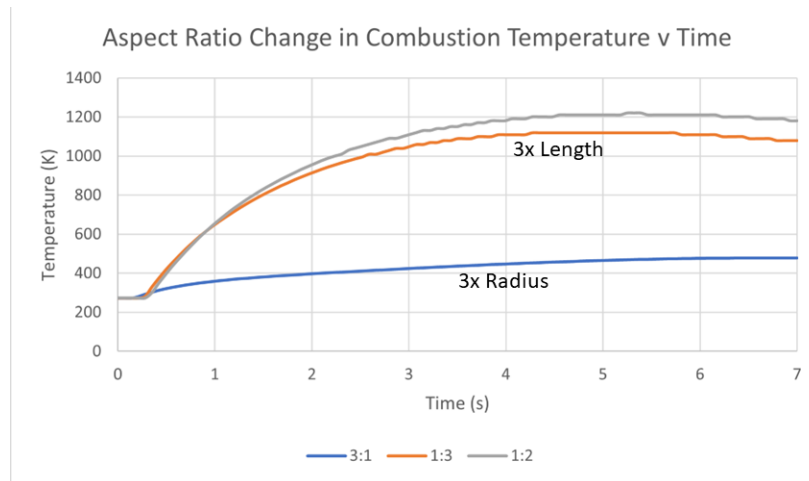


Figure 22: Aspect Ratio Change in Combustion Temperature Over Time

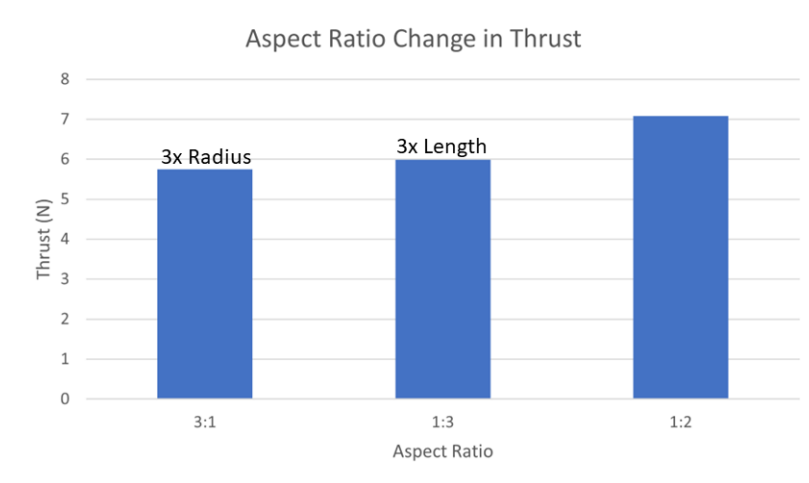


Figure 23: Aspect Ratio Change in Thrust

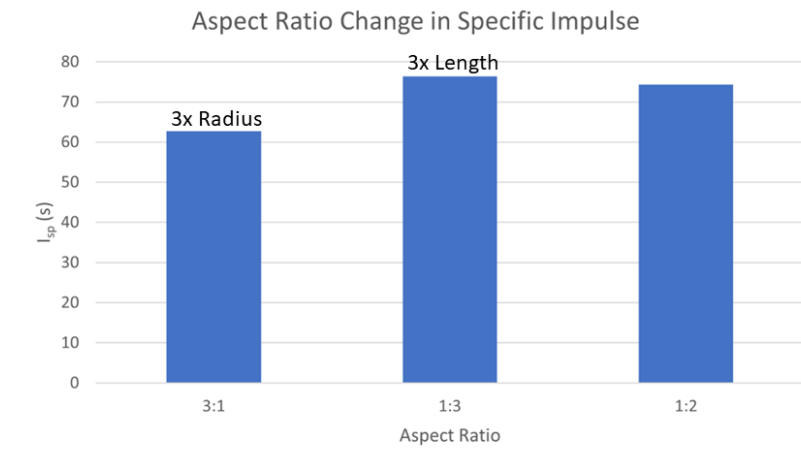


Figure 24: Aspect Ratio Change in Specific Impulse

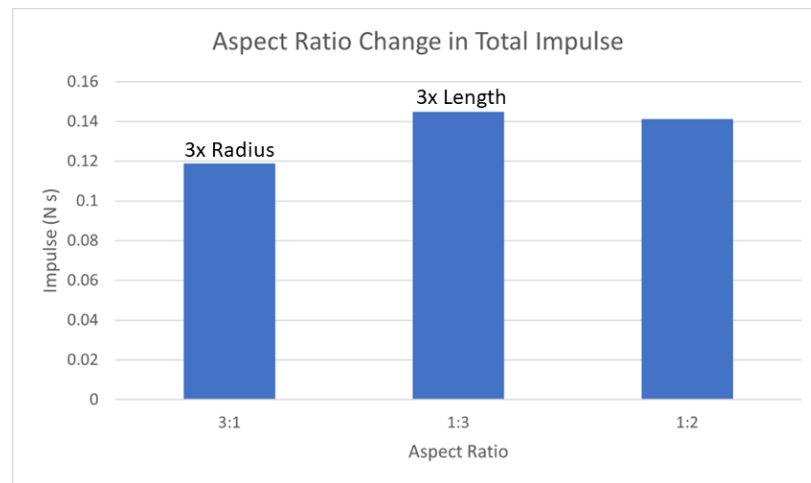


Figure 25: Aspect Ratio Change in Total Impulse

Figure 24 and Figure 25 indicate that the combustion chamber with the length longer than the radius, or pill-shaped (1:3), will have slightly higher specific and total impulse values than the spherical chamber (1:2). The pill-shaped chamber will also have a higher specific

and total impulse than the chamber with a longer radius than length, or disk-shaped (3:1). The spherical combustion chamber will still outperform both configurations regarding thrust, due to the chamber walls forcing the combustion gases closer together, producing a larger chamber pressure as shown by Figure 21. The greatest difference between chamber configurations, however, is seen in Figure 22 where the pill-shaped combustion chamber temperature nearly meets the spherical chamber while the disk-shaped chamber results in lower combustion temperatures. This is due to the fact that the combustion process takes place in the center of the combustion chamber and results in the temperature not being able to reach the far walls as it does with the other two configurations.

Figure 26 through Figure 30 show the last test of changing the power applied to the Nichrome wire. The same combustion chamber used by the Senior Design team was used for these tests. This chamber has an aspect ratio of 1:3 and a volume of 250 cm³.

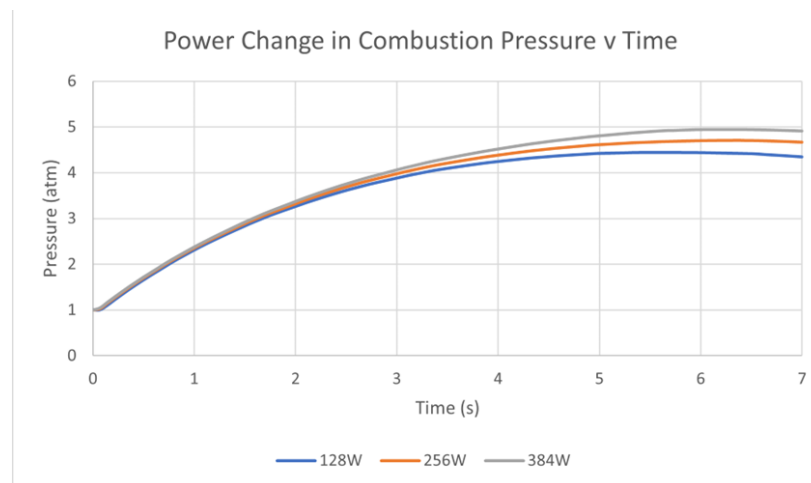


Figure 26: Power Change in Combustion Pressure Over Time

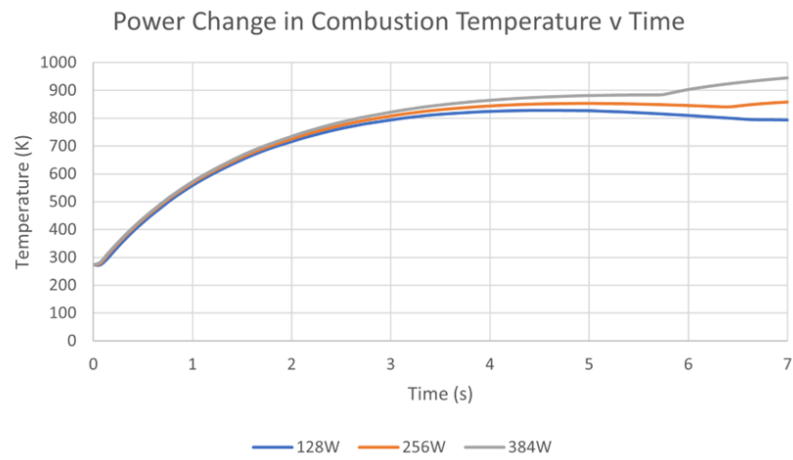


Figure 27: Power Change in Combustion Temperature Over Time

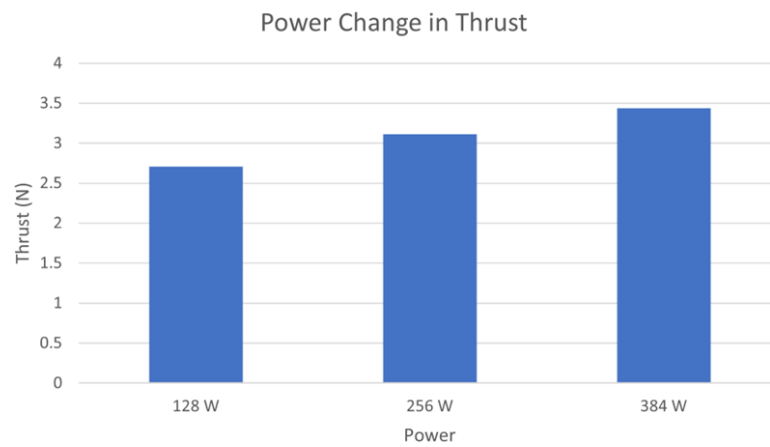


Figure 28: Power Change in Thrust

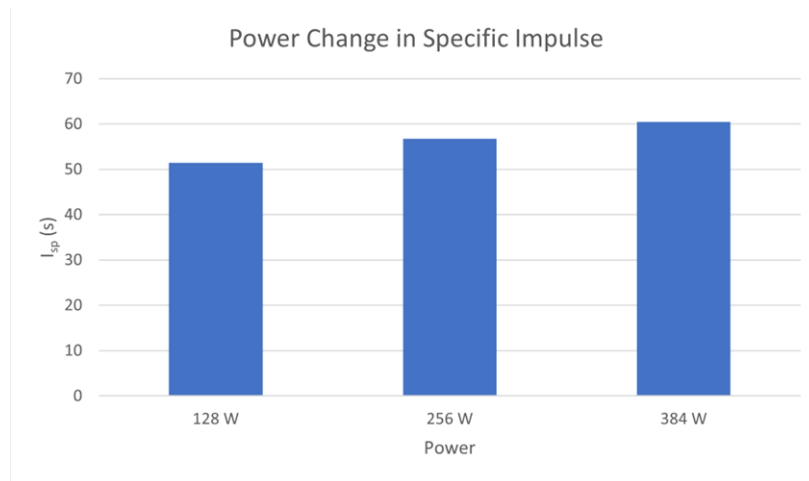


Figure 29: Power Change in Specific Impulse

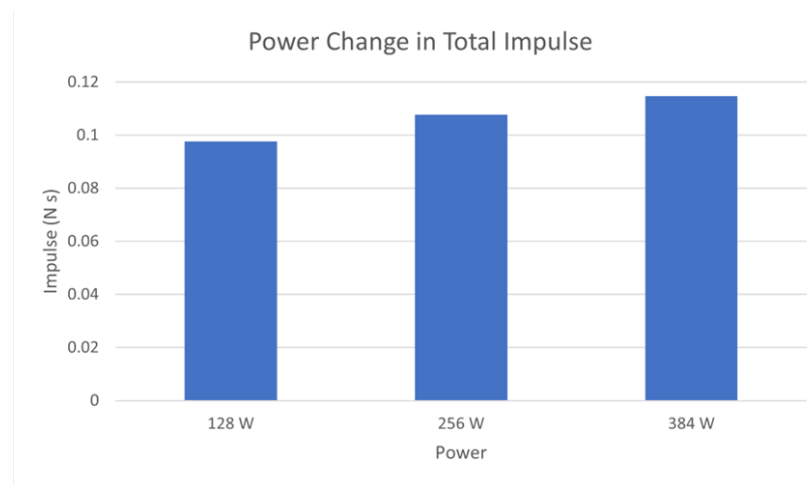


Figure 30: Power Change in Total Impulse

Figure 28, Figure 29, and Figure 30 show that the thrust, specific impulse, and total impulse increase with the power applied to the Nichrome wire. Figure 26 and Figure 27 display that the pressures and temperatures for each wire are around the same values before

they vary toward the end. Based on these graphs, changing the power to the wire has a greater effect on the combustion temperature than it does on the pressure, resulting in relatively small changes to the thrust, specific impulse, and total impulse.

Chapter 5

Conclusion

Conclusion

Based on the simulated results, the optimal propellant to use to increase the thrust, total impulse, and specific impulse of the CubeSat is the 50/50 Nitroglycerin/Nitrocellulose propellant. This propellant will supply 6.93 N of thrust with a specific impulse of 95.59 s and a total impulse of 0.17 N·s. For optimal results, a spherical combustion chamber with a small volume should be used. However, using a combustion chamber that has a longer length than radius (pill-shaped) will give similar results and is able to be manufactured easier than the spherical chamber. In terms of applying power to the Nichrome wire, applying more power to the wire will produce slightly higher values. This increased power could in turn aid in the burning process of the propellant and lead to shorter burn times. These phenomena would occur because the higher power to the wire enables the wire to reach higher temperatures, causing the propellant to combust faster.

Recommendations/Future Work

To validate the results of this work further, the full version of Flow-3D® should be purchased in order to allow for more tests to run at a time. This will enable finer meshes to be used and increase the accuracy of each test. Additionally, a combustion chamber based on the suggestions listed should be manufactured and tested with the 50/50 Nitroglycerin/Nitrocellulose propellant. The chamber should also be tested in a vacuum chamber to simulate the space environment.

Furthermore, the combustion properties of more solid propellants should be tested and found through experiments to allow for consistent simulation modeling. With consistent burning rate data, the calculated results will become more consistent and accurate.

References

- [1] Brief History of Rockets. https://www.grc.nasa.gov/www/k-12/TRC/Rockets/history_of_rockets.html. Accessed Nov. 30, 2021.
- [2] Thomas, J. C., Rodriguez, F. A., Sammet, T., Dillier, C. A., Petersen, E. D., and Petersen, E. L. Manufacturing and Burning of Composite AP/HTPB/AP Laminate Propellants. Presented at the AIAA Propulsion and Energy 2019 Forum, Indianapolis, IN, 2019.
- [3] Northway, P., Aubuchon, C., Mellema, H., Winglee, R., and Johnson, I. Pulsed Plasma Thruster Gains in Specific Thrust for CubeSat Propulsion. Presented at the 53rd AIAA/SAE/ASEE Joint Propulsion Conference, Atlanta, GA, 2017.
- [4] Kanchwala, T. “Feasibility Analysis and Performance Study of a Pulsed Solid Propellant Integrated Propulsion System for Small Satellites.” 2021, p. 133.
- [5] Dillier, C., Demko, A. R., Thomas, J. C., Grossman, K., Seal, S., and Petersen, E. L. Evaluation of Composite Propellants Utilizing Various Nano-Scale Aluminum and Boron Incorporation Methods. Presented at the AIAA Scitech 2019 Forum, San Diego, California, 2019.
- [6] Effects of Aluminum and Temperature on the Tensile Mechanical Properties of Lithium-Perchlorate/Polyvinyl Alcohol-Based Electrically Controlled Solid Propellants. <https://onlinelibrary-wiley-com.portal.lib.fit.edu/doi/epdf/10.1002/prep.201900281>. Accessed Nov. 14, 2021.
- [7] ANSYS FLUENT 12.0 User’s Guide - 16.4.5 Modeling Coal Combustion Using the Non-Premixed Model. <https://www.wfs.portici.enea.it/project/neptunius/docs/fluent/html/ug/node560.htm>. Accessed Apr. 17, 2022.
- [8] View of Investigation of Solid Propellant Rocket Motor Nozzle via CFD Simulation. <https://akademiabaru.com/submit/index.php/arfmts/article/view/3559/2577>. Accessed Mar. 14, 2022.
- [9] Bougamra, A., and Lu, H. “Multiphase CFD Simulation of Solid Propellant Combustion in a Small Gun Chamber.” *International Journal of Chemical Engineering*, Vol. 2014, 2014, pp. 1–10. <https://doi.org/10.1155/2014/971808>.
- [10] OpenFOAM: User Guide: Combustion. <https://www.openfoam.com/documentation/guides/latest/doc/guide-applications-solvers-combustion.html?msclkid=88ec6532beae11ec832a246a878c3ef0>. Accessed Apr. 17, 2022.
- [11] Konečný, P., and Ševčík, R. “Comparison of Turbulence Models in OpenFOAM for 3D Simulation of Gas Flow in Solid Propellant Rocket Engine.” *Advances in Military Technology*, Vol. 11, No. 2, 2016, pp. 239–251. <https://doi.org/10.3849/aimt.01131>.
- [12] Retief, F., Knoetze, J., Rousseau, C. W., Steenkamp, A. J., and Smit, G. J. A Comparison between the OpenFOAM® Toolbox and Custom-Built Numerical Solvers for Composite Solid Propellant Combustion Modeling. Presented at the 49th AIAA/ASME/SAE/ASEE Joint Propulsion Conference, San Jose, CA, 2013.

- [13] Gariani, G., Maggi, F., and Galfetti, L. “Numerical Simulation of HTPB Combustion in a 2D Hybrid Slab Combustor.” *Acta Astronautica*, Vol. 69, Nos. 5–6, 2011, pp. 289–296. <https://doi.org/10.1016/j.actaastro.2011.03.015>.
- [14] *Flow-3D® Version 22.1*. Flow Science, Inc., Santa Fe, NM, 2021.
- [15] *Flow-3D® Version 21.1 Users Manual*. Flow-3D, , 2022.
- [16] Cai, W., Thakre, P., and Yang, V. “A Model of AP/HTPB Composite Propellant Combustion in Rocket-Motor Environments.” *Combustion Science and Technology*, Vol. 180, No. 12, 2008, pp. 2143–2169. <https://doi.org/10.1080/00102200802414915>.
- [17] Lengellé, G., Duterque, J., and Trubert, J. F. “Combustion of Solid Propellants.” p. 63.
- [18] Woo, J., Cha, S.-W., Kim, G., Kim, J. H., Roh, T.-S., Cho, J. Y., Jang, S.-G., Lee, H.-N., and Yang, H. W. “Concept of Unburning Ratio and Combustion Modeling of ZPP and BKNO₃ in Pyroshock-Reduced Separation Nut.” *Propellants, Explosives, Pyrotechnics*, Vol. 45, No. 5, 2020, pp. 775–787. <https://doi.org/10.1002/prep.201900255>.
- [19] Varney, A. M., and Martino, J. “Expanded Ignition Effectiveness Tests of Selected Igniter Materials with Navy Propellants.” p. 133.
- [20] Rozumov, D. E., Park, D., Manning, T., O’Reilly, J., Laquidara, J., and Thompson, D. “High Performance BKNO₃ Igniter Formulations.” 2009, p. 26.
- [21] Dennis, C., and Bojko, B. “On the Combustion of Heterogeneous AP/HTPB Composite Propellants: A Review.” *Fuel*, Vol. 254, 2019, p. 115646. <https://doi.org/10.1016/j.fuel.2019.115646>.
- [22] Shi, X., Jia, Y., Chen, L., Tian, L., Shen, J., and Pei, C. “Tuning the Laser Ignition Properties of Nitrocellulose-Nitroglycerine-Hexogen Propellants via Incorporation of Carbon Nanotubes.” *Central European Journal of Energetic Materials*, Vol. 18, No. 3, 2021, pp. 385–404. <https://doi.org/10.22211/cejem/142604>.
- [23] 304 Stainless Steel. *304 Stainless Steel*. <https://304stainlesssteel.org/>. Accessed Apr. 18, 2022.
- [24] Nichrome Wire. <https://temcoindustrial.com/product-guides/wire-cable-and-accessories/resistance-and-non-resistance-wire/nichrome-wire>. Accessed Apr. 18, 2022.
- [25] Nichrome Wire-Nichrome 80 Wire, Nichrome 60 Wire. Heanjia Super Metals Co. Ltd.
- [26] Staley, C. S., Raymond, K. E., Thiruvengadathan, R., Apperson, S. J., Gangopadhyay, K., Swaszek, S. M., Taylor, R. J., and Gangopadhyay, S. “Fast-Impulse Nanothermite Solid-Propellant Miniaturized Thrusters.” *Journal of Propulsion and Power*, Vol. 29, No. 6, 2013, pp. 1400–1409. <https://doi.org/10.2514/1.B34962>.

Appendix

Matlab Code

```
% Timothy Aaron Blackman
% CubeSat Thruster Calculations

clear all; close all; clc;

% Engine Geometry
% Nozzle
noz = 0.005895; % (m)
noz = (pi/4)*noz*noz; % (m2)
ang = 8; % Half Angle (deg)

% Throat Area
throat = 0.003151; % (m)
throat = (pi/4)*throat*throat; % (m2)

area_rat = noz/throat;

% Read in data from Flow3D
prompt = 'What is the name of the Flow3D csv file?';
str = input(prompt,'s');
str_in = insertAfter(str,str, ".csv");
filename =
fullfile('C:\Users\Owner\Documents\MATLAB\Grad\Thesis\Props',str_in
);
inputdata = readtable(filename);

% Propellant data
rho_p = table2array(inputdata(1,1)); % (kg/m3)
A = table2array(inputdata(1,2)); % (cm/s)
n = table2array(inputdata(1,3)); % Burn Rate Exponent
cp = table2array(inputdata(1,4)); % (J/kg K)

vol = (4/3)*pi*(.003^3); % (m3)
mass = rho_p*vol;

% Remove propellant data from chamber data
inputdata(1,:) = [];

% Chamber data
p = table2array(inputdata(:,1)); % (Pa)
rho = table2array(inputdata(:,2)); % (kg/m3)
T = table2array(inputdata(:,3)); % (K)
u = table2array(inputdata(:,4)); % (m/s)
time = table2array(inputdata(:,5)); % (s)

% Find the size of the pressure array
count = size(p,1);
```

```

% Gas Constants
rho_comb = rho(end); % (kg/m3)
p_max = max(p); % (Pa)
T_max = max(T); % (K)

R = p_max/(rho_comb*T_max); % (J/kg K)
gamma = (cp/R)/((cp/R)-1); % Specific Heat Ratio

% Combustion Calculations
p0 = 101300; % (Pa)
a_cc = sqrt(gamma.*R.*T(end)); % (m/s)
M_cc = u(end)./a_cc;
p0 = p(end).*(1+((gamma-1)/2).*M_cc.*M_cc).^(gamma./(gamma-1));
% (Pa)
To = T(end).*(1+((gamma-1)/2).*M_cc.*M_cc); % (K)

% Nozzle Choking Pressure Conditions
choke_rat=((gamma+1)/2).^(gamma./(gamma-1));
choke_press = p0.*choke_rat;
choke_chamb = choke_press./101300 % [atm]

% Solve Area Ratio for Mach
syms M
eq = (1./M).*((2./(gamma+1)).*(1+((gamma-1)/2).*M.*M)).^(gamma+1./(2.*(gamma-1)));
eq = eq == area_rat;
M = vpasolve(eq,M,2);
M = double(M);

% Nozzle Exit
pe = p0./((1+((gamma-1)/2).*M.*M).^(gamma./(gamma-1))); % (Pa)
Te = To./(1+((gamma-1)/2).*M.*M); % (K)
ae = sqrt(gamma.*R.*Te); % (m/s)
ue = M.*ae; % (m/s)
rhoe = pe./(R.*Te); % (kg/m3)
massflow = rhoe.*ue.*noz; % (kg/s)

% Thrust, Isp, Total Impulse Calculations
thrust = ((1+cosd(ang))./2).*massflow.*ue+(pe-p0).*noz % (N)
Sp_Isp = thrust./(9.81.*massflow) % (s)
Impulse = Sp_Isp.*mass.*9.81

% Prepare output tables. Thruster is designed for full combustion
of one
% pellet, so thrust, Isp, and I are only calculated at the ending
values of
% pressure and temperature.
for i=1:(count-1)
    t(i) = 0.0;
    Isp(i) = 0.0;
    I(i) = 0.0;
end

% Transpose thrust, Isp, and I vectors

```

```

t = t.';
Isp = Isp.';
I = I.';

% Input thrust, Isp, and I values
t(count) = thrust;
Isp(count) = Sp_Isp;
I(count) = Impulse;

% Export pressure in (atm)
p = p./101300;

% Output Thrust and Isp to csv file
str_out = insertAfter(str,str,"_results.xlsx");
filename =
fullfile('C:\Users\Owner\Documents\MATLAB\Grad\Thesis\Props',str_out);
t);
outputdata = table(time,p,T,t,Isp,I);
writetable(outputdata,filename);

```

Example Matlab Input File Data (80/20 AP/HTPB)

1710	0.0331	0.433	1740	0
101300	1.29	2.73E+02	0	0.00E+00
101318.3	1.29	2.73E+02	0.02	7.00E-02
110975.1	1.38	2.95E+02	3.89	1.40E-01
122708.9	1.48	3.23E+02	3.67	2.10E-01
134157.8	1.58	3.50E+02	3.29	2.80E-01
145282.4	1.67	3.75E+02	2.93	3.50E-01
155973	1.76	4.00E+02	2.63	4.20E-01
166198	1.84	4.22E+02	2.59	4.90E-01
176238	1.92	4.44E+02	2.45	5.60E-01
185825.2	2	4.64E+02	2.2	6.30E-01
195355.9	2.07	4.83E+02	2.2	7.00E-01
205126.8	2.14	5.03E+02	2.28	7.70E-01
214185.1	2.21	5.21E+02	1.91	8.40E-01
222838.6	2.28	5.37E+02	1.78	9.10E-01
231437.3	2.34	5.54E+02	1.63	9.80E-01
239669.6	2.4	5.69E+02	1.68	1.05E+00
247663.2	2.46	5.83E+02	1.5	1.12E+00
255267.6	2.51	5.97E+02	1.43	1.19E+00
262743.4	2.57	6.10E+02	1.55	1.26E+00

270022.2	2.62	6.22E+02	1.45	1.33E+00
277170.6	2.67	6.34E+02	1.41	1.40E+00
284218.6	2.71	6.46E+02	1.42	1.47E+00
291320.2	2.76	6.57E+02	1.45	1.54E+00
297908.5	2.8	6.67E+02	1.42	1.61E+00
304341.7	2.83	6.77E+02	1.29	1.68E+00
310640.4	2.85	6.87E+02	1.18	1.75E+00
316329.9	2.87	6.95E+02	1.09	1.82E+00
321910.5	2.88	7.03E+02	1.07	1.89E+00
327332.5	2.89	7.11E+02	1.04	1.96E+00
332861.3	2.89	7.19E+02	1.03	2.03E+00
338422.2	2.89	7.27E+02	1.02	2.10E+00
343569.4	2.88	7.34E+02	1.02	2.17E+00
348584.7	2.87	7.40E+02	1.11	2.24E+00
353535.9	2.86	7.47E+02	1.07	2.31E+00
358273.8	2.84	7.53E+02	1.11	2.38E+00
362919	2.83	7.59E+02	1.07	2.45E+00
367348.2	2.81	7.64E+02	1.12	2.52E+00
371512	2.79	7.69E+02	1.07	2.59E+00
375695	2.78	7.74E+02	1.02	2.66E+00
379720.2	2.76	7.79E+02	1.02	2.73E+00
383342.4	2.75	7.83E+02	0.96	2.80E+00
386856.5	2.73	7.86E+02	0.87	2.87E+00
390349.9	2.72	7.90E+02	0.87	2.94E+00
393902.4	2.71	7.94E+02	0.86	3.01E+00
397458.9	2.71	7.97E+02	0.85	3.08E+00
400757.6	2.7	8.01E+02	1	3.15E+00
403828.4	2.7	8.04E+02	1.03	3.22E+00
406900.9	2.69	8.07E+02	0.87	3.29E+00
409913	2.69	8.09E+02	0.83	3.36E+00
412527.2	2.69	8.12E+02	0.93	3.43E+00
414955.9	2.69	8.14E+02	0.91	3.50E+00
417298.1	2.68	8.15E+02	0.97	3.57E+00
419610.9	2.68	8.17E+02	0.92	3.64E+00
421837.8	2.68	8.19E+02	0.88	3.71E+00
424025.7	2.68	8.20E+02	0.85	3.78E+00
426190.7	2.68	8.22E+02	0.81	3.85E+00

428175.4	2.69	8.23E+02	0.82	3.92E+00
429935	2.69	8.24E+02	0.78	3.99E+00
431648	2.69	8.25E+02	0.78	4.06E+00
433337.8	2.69	8.25E+02	0.72	4.13E+00
435030.5	2.69	8.26E+02	0.79	4.20E+00
436611.1	2.69	8.27E+02	0.76	4.27E+00
438169.7	2.69	8.27E+02	0.74	4.34E+00
439481.4	2.69	8.27E+02	0.75	4.41E+00
440651	2.69	8.27E+02	0.81	4.48E+00
441962.4	2.69	8.28E+02	0.86	4.55E+00
443064	2.69	8.28E+02	0.87	4.62E+00
444046.2	2.69	8.28E+02	0.88	4.69E+00
445016.9	2.69	8.27E+02	0.81	4.76E+00
445975.4	2.69	8.27E+02	0.77	4.83E+00
446951.2	2.69	8.27E+02	0.73	4.90E+00
447909	2.69	8.27E+02	0.72	4.97E+00
448367.2	2.69	8.26E+02	0.72	5.04E+00
448631.2	2.69	8.25E+02	0.7	5.11E+00
448976	2.69	8.24E+02	0.69	5.18E+00
449383.5	2.69	8.23E+02	0.7	5.25E+00
449831.6	2.68	8.22E+02	0.72	5.32E+00
450095	2.68	8.21E+02	0.77	5.39E+00
450117	2.68	8.20E+02	0.69	5.46E+00
450146.6	2.68	8.19E+02	0.67	5.53E+00
450270.6	2.67	8.17E+02	0.85	5.60E+00
450263.5	2.67	8.16E+02	0.77	5.67E+00
450180.9	2.67	8.15E+02	0.74	5.74E+00
450101	2.67	8.13E+02	0.72	5.81E+00
450000.1	2.66	8.12E+02	0.72	5.88E+00
449893.8	2.66	8.11E+02	0.74	5.95E+00
449709.7	2.66	8.09E+02	0.69	6.02E+00
449408.9	2.65	8.07E+02	0.68	6.09E+00
449055.6	2.65	8.06E+02	0.67	6.16E+00
448755.3	2.65	8.04E+02	0.67	6.23E+00
448432.4	2.64	8.02E+02	0.66	6.30E+00
448132.1	2.64	8.01E+02	0.65	6.37E+00
447819.1	2.64	7.99E+02	0.65	6.44E+00

447426.1	2.63	7.98E+02	0.73	6.51E+00
446595	2.63	7.96E+02	0.7	6.58E+00
445351.6	2.62	7.94E+02	0.67	6.65E+00
444464.9	2.62	7.94E+02	0.61	6.72E+00
443526.5	2.61	7.94E+02	0.57	6.79E+00
442537.2	2.61	7.94E+02	0.54	6.86E+00
441496.1	2.61	7.94E+02	0.53	6.93E+00
440410.3	2.6	7.93E+02	0.51	7.00E+00